Light Scattering from Dilute Polymer Solutions in Shear Flow

Alfred Link and Jürgen Springer*

Fachgebiet Makromolekulare Chemie, Institut für Technische Chemie, Technische Universität Berlin, Strasse des 17.Juni 135, W-1000 Berlin 12, Germany

Received December 30, 1991; Revised Manuscript Received September 22, 1992

ABSTRACT: A self-constructed laser light scattering photometer including a shear cell has been used to investigate the scattering behavior of polystyrene ($M_W = 10.3 \times 10^6$) in the viscous solvent dioctyl phthalate (DOP) in shear flow. Only highly dilute solutions were used ($c < 0.8/[\eta]$). Changes of the scattering intensity were detected, depending on shear rate, detection angle, and polymer concentration. The special feature of our instrument is its ability to detect the scattering intensity in the plane of flow as well as in several planes perpendicular to the flow plane (Zimm planes). From measurements in the flow plane, the orientation angle can be determined directly. Furthermore, by variation of the wavelength of the incident light and detection angle, all three main radii of the ellipsoidal gyration space of polymer coils in shear flow were determined. While the orientation angles obtained show at least qualitative coincidence with the dynamic theories of Rouse and Zimm, a large discrepancy between theoretical and experimental molecular deformation was observed. The maximum deformation ratio of the radius of gyration compared to quiescent solution was 1.5. We also noticed a pronounced dependence of the orientation angle and deformation ratio on concentration. Additionally, in the polymer–solvent system considered, a shear-induced phase separation was encountered.

Introduction

The knowledge of the behavior of single polymer molecules in flow can give new insights into polymer physics, in addition to the industrial interest in phenomena such as drag reduction or high-performance polymer fiber spinning from dilute solution. In the last years, some interest has been taken in polymers subjected to flow by various methods.[1] Basically, only scattering methods are able to give direct information about the dimensions of polymer molecules. Due to experimental difficulties arising from the combination of a flow cell with light scattering optics and the combined rheological and optical conditions that must be met, very few investigations in this field have been published.[2-8] We present measurements of wide-angle light scattering (LS) from dilute polystyrene solutions in shear flow.

Macromolecules are usually characterized by size measures such as the gyration radius $\langle r_{gyr}^2 \rangle^{1/2}$ which can be determined by scattering methods. Theoretical calculations of the shape of single macromolecules are not available, but it was shown by Monte Carlo simulations that a random coil is not a sphere but has an ellipsoidal shape characterized by three coil main radii.[9]

In quiescent solution, no information about the coil radii is yielded because, due to the Brownian rotation of the coil molecules and comparatively large experimental scattering volumes, only the spherical shape of the enveloping volume (i.e., the gyration space) of the molecules is observed by LS. On application of a shear rate of at least the same order of magnitude as the rotatory diffusion constant of the particles, nonuniform rotation (orientation) and molecular deformation occur simultaneously in the plane of flow.[10] Both effects cause a change of the spherical gyration space of the molecules into a gyration ellipsoid with three main gyration radii. These have been measured in the present work.

Predictions about the orientation and deformation of polymer molecules in solution are made by the basic dynamic polymer models: Kuhn[11] (elastic dumbbell model), Rouse[12] (spring–bead model), and Zimm models[13] (spring–bead model including hydrodynamic interactions of the beads). These are widely accepted though important properties of polymer solutions such as the shear rate dependence of the dilute solution viscosity are not explained. The theories predict that orientation and deformation take place if the longest relaxation time of the molecules multiplied by the shear rate is greater than 1. Orientation causes a viscosity drop, whereas a molecular extension should raise the solution viscosity. The two effects are predicted to compensate exactly, in obvious contrast to reality.

However, the theoretical results lead to the formulation of the dimensionless shear parameter (or reduced shear rate) β. If $\beta \geq 1$, shear effects on polymer molecules in dilute solution can be expected.

$$\beta = \left[q\frac{(\eta - \eta_0)M}{cRT}\right]_{c>0} = \left[q\frac{[\eta]\eta_0 M}{RT}\right]_{c\to 0} \qquad (1)$$

$q = -\mathrm{d}v_x/\mathrm{d}y$ is the flow velocity gradient, η denotes the dynamic viscosity, and η_0 is the viscosity of the solvent. $[\eta]$ is the intrinsic viscosity, M the molecular mass, and c the mass concentration of polymer. R and T denote the gas constant and absolute temperature, respectively.

It was recognized by Peterlin, Heller, and Nakagaki[14-17] that light scattering should be a useful tool to investigate the conformation of macromolecules in shear flow. They developed methods to evaluate LS measurements of sheared polymer solutions. Using these procedures, we can determine the orientation angle of polymer molecules in shear flow as well as all three independent main radii of the molecular gyration space, as a function of shear rate.

Streaming birefringence is a related method with which the orientation of macromolecules can also be determined directly. However, this method is restricted to polymer–solvent systems that show low depolarization in quiescent solution, i.e., systems that have no (or low) scattering intensity contrast. For LS of flowing solutions, exactly the opposite condition is required. Additionally, streaming birefringence yields no information about the conformation except for an estimation of the change of the mean-square end-to-end distance $\langle R_e^2 \rangle$ with flow, based on several assumptions.[18] Compared to that, LS is able to give detailed information about each of the main gyration radii in flow, with almost no assumptions.

Elongational flow is expected to cause a much higher molecular deformation. Some experimenters[19-22] used light scattering to investigate polymers in transient

0024-9297/93/2226-0464$04.00/0

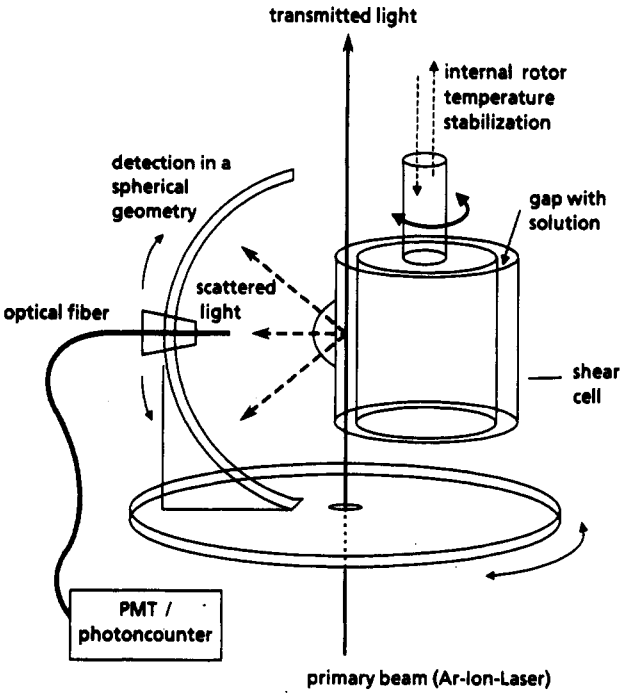

Figure 1. Experimental setup. The optical fiber end can be moved horizontally and vertically.

elongational flow, but this is difficult to control, and an important open question is whether the molecules spend enough time in the stagnation point to be stretched as predicted.[22] In contrast, shear flow has advantages. It can be controlled easily, and the scattering volume is not critical, due to the fact that, for example, in a double cylinder shear cell, all molecules of the cell volume are subjected to approximately the same shear rate throughout the experiment.

We present quantitative measurements of the molecular orientation and deformation of single polymer molecules in shear flow. We use a "static" laser light scattering apparatus including a shear cell, allowing measurements in the flow plane and various "Zimm planes" (i.e., detection planes containing the primary beam; see below). The determination of orientation angles together with all three independent main gyration radii of polymer molecules in sheared solution is presented for the first time.

Experimental Section

A laser light scattering photometer was used combined with a Searle-type shear cell with a rotating inner cylinder. It allows lateral detection of the scattered light not only in one plane as usual but in a hemispherical geometry (Figure 1).

Therefore, the flow plane, which is defined by the vectors of flow velocity and velocity gradient, is accessible as well as various Zimm planes, which contain the primary beam. This is the most important experimental difference between this work and all comparable publications by other authors (Figure 2).

The orientation angle χ is defined as the angle between the longest gyration space axis and the flow velocity direction. The setup is attached to a 2-m optical double rail (Spindler & Hoyer, Germany), set on a self-constructed vibration-reducing table. The intensity-stabilized primary laser beam (Ar ion laser Model 2025-05; Spectra-Physics, San Jose, CA) passes through a polarizer rotator and is focused by an achromatic lens (f = 300 mm) to a diameter of approximately 0.5 mm in the scattering cell. The irradiated power is approximately 100 mW; the primary beam is always vertically polarized in relation to ω. The incident light passes upward through the gap between the cylinders (1.0 mm), parallel to the rotor axis. Having passed the cell, the transmitted light is measured by a photodiode.

The outer cylinder of the shear cell and the bottom and cap plates are made of optical glass (Heraeus, Germany), while the

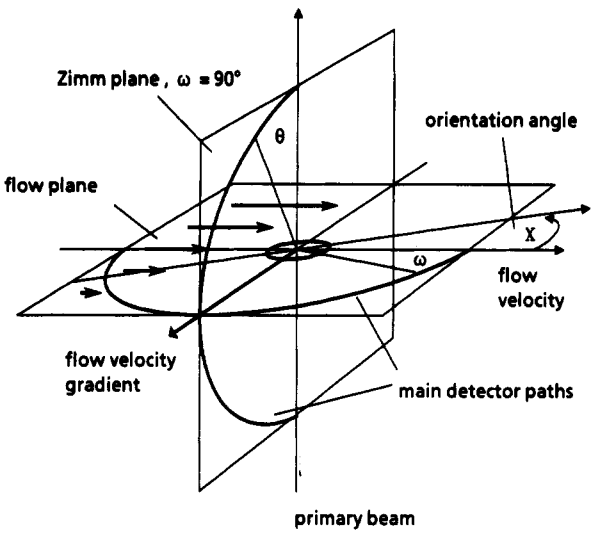

Figure 2. Detection geometry including the detection angles ω and θ in the flow plane and Zimm planes, respectively.

inner cylinder is made of nickel-plated, chromium-blackened brass (diameter 58 mm).[23] The cell is sealed by Teflon and Viton rings. Approximately 20 mL of solution are required. To reduce scattering intensity errors due to refractive index differences between the cylindrical outer glass wall and the surrounding air, a spherical lens is glued onto the outer cylinder.[23]

The hemispherical detection geometry is formed by a horizontal rotational stage (Model 410, Huber, Germany) and a self-constructed vertical hemicircular guide rail which leads the optical fiber (Quartz & Silice, France). The scattering intensity measurements were done by photo counting (photon counter 5C1, EG&G Brookdeal). No polarization analyzer was used. The resolution of the fiber optics is 37×10^{-6} sr, ie., the scattering volume is approximately $0.3/\sin\theta$ mm^3.

Because of the low thermal conductivity of optical glass, the hollow rotating inner cylinder is passed by thermostated water, keeping it at constant temperature to within ±0.05 °C, independent of shear rate and solution viscosity (η = 1–200 mPa s). The rotor is driven by a stepper motor with microstep control to assure uniform movement (Franke CNC, Germany). The maximum shear rate is 2000 s^{-1}.

Stress data cannot be recorded from the rotor; the viscosity behavior of all solutions was checked before and after the scattering experiments by an external viscometer (CV100, Haake, Germany). Even in the laminar flow regime, the occurrence of secondary flows such as Taylor vortices was taken into account. Consideration of these effects limits the maximum shear rate of the simple laminar flow regime; see the Materials section.

All movements and intensity measurements are monitored by a PC. The maximum angular detection range is 30–150° for both angles ω and θ. In addition to some other criteria, the setup was checked for the Rayleigh scattering of toluene which was found to be correct within ±5% in the ranges of ω = 40–140° and θ = 35–120°. Reading time was 100 ms; all data points shown below are averages of 50–100 primary values. The count rate for toluene (vertically polarized, 90°/90°) is 3550 ± 80 with a dark count rate of 2. Polymer concentration was chosen to give at least 200% of the solvent scattering at θ = 120°.

Materials. As flow light scattering combines two experiments, the experimental conditions for both must be met. On the one hand, high molecular weight polymers and highly viscous solvents are required to reach $\beta \geq 1$ (eq 1), and stable laminar flow has to be assured. On the other hand, the most important condition for a light scattering experiment is a sufficient refractive index increment.

Therefore, for all investigations a polystyrene (PS) standard of $M_W = 10.3 \times 10^6$, $M_W/M_N = 1.25$ (Polymer Laboratories, U.K.) was used ("PS10"). Diethylhexyl phthalate (dioctyl phthalate, DOP) was found to have the desired properties at 25 °C: dynamic viscosity η = 61 mPa s, refractive index increment of PS in DOP dn/dc (514 nm) = 0.119 mL/g, intrinsic viscosity $[\eta]_{10.3}$ = 260 cm^3/g, determined by extrapolations $c \to 0$ and $q \to 0$, i.e., the

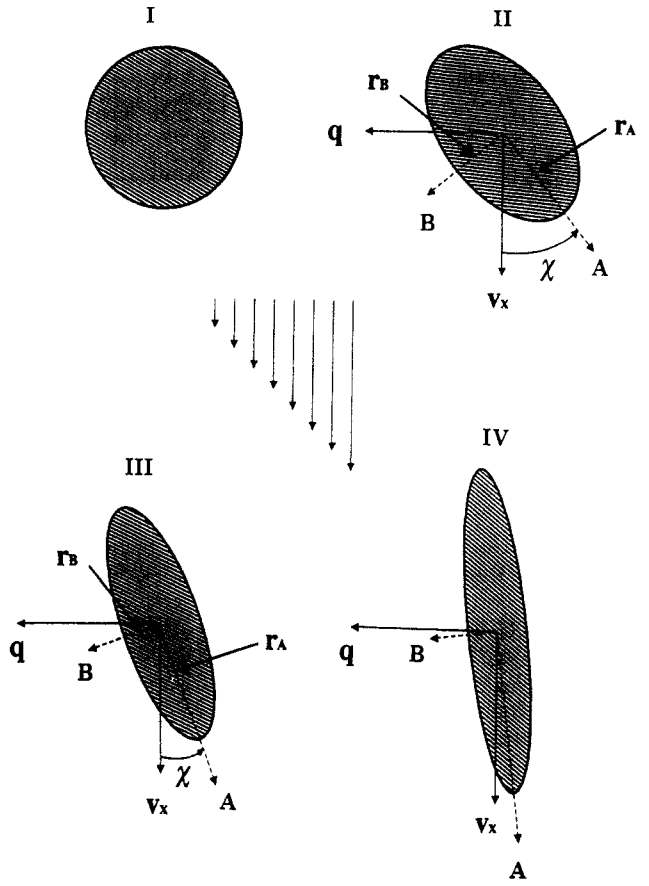

Figure 3. Theoretical estimation of the gyration space radii r_A and r_B of coil molecules in increasing shear flow (I–IV).

Schurz procedure.[24] In the following, all values of the shear parameter β were calculated according to eq 1 using the previously determined viscosity data. The overlap concentration was estimated to be $c^* = 1/[\eta] \approx 3.8$ g/L; the highest concentration used was $0.75c^*$. Prior to and after the rheooptical measurements, the scattering behavior was checked in a conventional LS photometer (Fica 50, France), where the nominal M_W was confirmed to within 10%.

LS at rest and viscosity measurements of several PS molecular mass standards clearly revealed that DOP at 25 °C is a near-Θ solvent for PS: $A_2 = 3.8 \times 10^{-5}$ cm³ mol/g²; the Mark–Houwink exponent is $a = 0.54$. The critical shear rate for the appearance of Taylor vortices in DOP at 25 °C can be calculated[25] to be approximately 14 000 s^{-1}, which is far beyond the shear rates used in this study ($q_{max} = 2000$ s^{-1}).

Sample Preparation. DOP (E. Merck, Germany) was filtered through 0.2-μm filters prior to solution preparation. Shaking and increased temperature (50–55 °C) are necessary to dissolve PS10 in 2–4 weeks. However, since degradation was observed in our first tests, great care was taken in the dissolution process later on; e.g., shaking was reduced to low frequencies and was applied only twice a day for several minutes. Before the scattering measurement, each solution was centrifuged at 3000g for 1 h and was filled with a syringe through a Teflon capillary into the scattering cell.

Theory

As already mentioned above, due to the fast Brownian rotation and a comparatively large scattering volume in quiescent solution only an averaged size measure, the radius of gyration, can be yielded. Under shear reaching $\beta > 1$, the molecular rotation becomes nonuniform, i.e., the enveloping volume of the particle becomes ellipsoidal. The longest main radius (r_A) of the deformed gyration space shows the preferential orientation. The angle between the flow velocity vector and the preferential direction is the orientation angle χ. The second radius

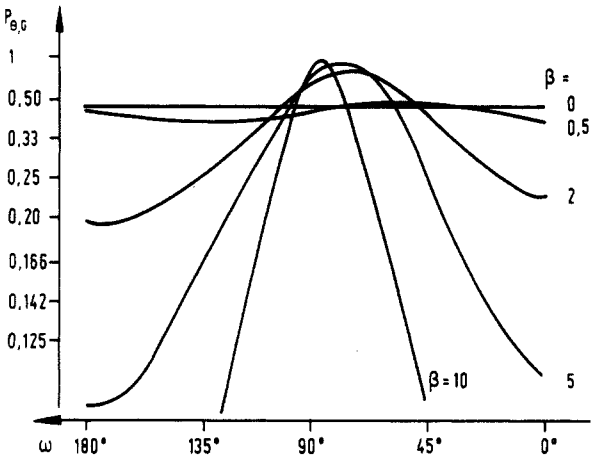

Figure 4. Peterlin scattering function for the elastic dumbbell model under shear in the flow plane for various shear parameters β.[14,15]

(r_B) in the flow plane should decrease while the third radius (r_C) should theoretically remain constant, because no velocity gradient acts in this direction[26] (Figure 3).

Orientation. Peterlin showed the theoretical scattering behavior of a polymer solution submitted to shear.[14–16,18] Numerical evaluation of his scattering functions based on the elastic dumbbell model and the Rouse model reveals a change of the scattered light distribution in the flow plane: in certain angle regions the scattering intensity is increased, and at other angles decreasing intensity is predicted with increasing shear rate (Figure 4).

Later, Nakagaki and Heller[17] calculated similar curves for rigid ellipsoids in shear flow, plotting the relative intensity (compared to rest) versus the detection angle ω. In both cases one gets sinusoidal curves showing a distinct maximum between $\omega = 45°$ and 90°. With increasing β the location of the maximum ω_{max} moves toward 90° while the amplitude increases. This reflects directly the decreased radius r_B of the gyration space of the molecules which results in increased local scattering intensity. Therefore the orientation angle can be easily calculated after determination of ω_{max}:

$$\chi = 90° - \omega_{max} \tag{2}$$

The dynamic models of Kuhn, Rouse, and Zimm predict

$$\chi = (1/2) \arctan (m/\beta) \tag{3}$$

with

$$m = 1 \text{ (Kuhn model)}^{11}$$

$$m = 2.5 \text{ (Rouse model)}^{12}$$

$$m = 4.88 \text{ (Zimm model)}^{13}$$

Deformation. Both rigid particles and random coils can be oriented in shear flow, but the latter will also show shear-induced deformation, i.e., extension of the mean radius of gyration. For LS evaluation, usually the Zimm approximation of the Debye scattering function for particles of any shape is used:

$$P(h) = 1 - \frac{h^2}{2N^2} \sum_k^N \sum_l^N \langle r_{kl,h}^2 \rangle + \ldots \tag{4}$$

$$P(h) = 1 - h^2 \langle S^2 \rangle + \ldots \tag{5}$$

$\langle S^2 \rangle$ being the mean-square correlation length

$$\langle S^2 \rangle = \frac{1}{2N^2} \sum_{k}^{N} \sum_{l}^{N} \langle r_{kl,h}^2 \rangle \quad (6)$$

where $h = |\mathbf{h}|$ = absolute value of the scattering vector = $(4\pi/\lambda) \sin(\theta/2)$, N = number of chain segments, and $\langle r_{kl,h}^2 \rangle$ = mean-square projection of the segment distance vector $\mathbf{r}_{kl}$ on $\mathbf{h}$.

In quiescent solution, the mean-square radius of gyration $\langle r_{gyr}^2 \rangle$ can be determined by the classical Zimm method performing angle variation and plotting P^{-1} vs $\sin^2(\theta/2)$ after $\langle r_{gyr}^2 \rangle = 3\langle S^2 \rangle$ (including extrapolations $c \to 0$ and $h \to 0$) because the correlation length $\langle S^2 \rangle^{1/2}$ is constant in all observation directions.

If the molecules are oriented (and eventually deformed) in a flow velocity gradient, their gyration space will be deformed from a sphere to an ellipsoid. The three main radii of this ellipsoid cannot be determined by angle variation in a Zimm plane and evaluation as usual, because, at each detection angle, a different correlation length determines the local scattering intensity. This leads to strongly curved Zimm plots $Kc/R(h)$ versus h^2 (K denotes the optical constant and $R(h)$ the reduced scattering intensity), and the extrapolated resulting values are therefore uncertain. An example will be shown below (Figure 10).

Unfortunately, no analytically applicable scattering function for oriented, deformed macromolecules is available. For the determination of the radius of gyration in shear flow, all three main correlation lengths $\langle S_A^2 \rangle^{1/2}$, $\langle S_B^2 \rangle^{1/2}$, and $\langle S_C^2 \rangle^{1/2}$ of the ellipsoidal gyration space must be known since the radius of gyration is

$$\langle r_{gyr}^2 \rangle = \langle S_A^2 \rangle + \langle S_B^2 \rangle + \langle S_C^2 \rangle \quad (7)$$

After a proposal of Peterlin,[14] the determination of the main correlation lengths can be performed by variation of the incident wavelength at a constant detector position, using the simple scattering function of Zimm. While the detector position remains unchanged, a complete Zimm scan can be performed by wavelength variation. In addition, this procedure has the advantage of being widely independent of assumptions concerning the shape of the scattering particles. These data are evaluated corresponding to eq 5. $\langle S^2 \rangle$ is then the mean-square, local correlation length of the gyration space in the direction of the scattering vector. In our case (Figure 2), it can be shown that $\langle S^2 \rangle$ can be described as

$$\langle S^2 \rangle = \langle S_A^2 \rangle (\cos^2(\theta/2) \cos^2 \omega') + \langle S_B^2 \rangle (\cos^2(\theta/2) \sin^2 \omega') + \langle S_C^2 \rangle (\sin^2(\theta/2)) \quad (8)$$

with $\omega' = \omega + \chi$.

From $\langle S^2 \rangle$ data of at least three detector positions, the three unknown quantities $\langle S_A^2 \rangle$, $\langle S_B^2 \rangle$, and $\langle S_C^2 \rangle$ can be calculated for each value of β, considering the respective orientation angle χ. Hence, $\langle r_{gyr}^2 \rangle$ can be easily calculated from eq 7.

The theoretical predictions for the deformation ratio of polymers in shear flow are

$$\langle r_{gyr}^2 \rangle / \langle r_{gyr,0}^2 \rangle \approx \langle R_e^2 \rangle / \langle R_{e,0}^2 \rangle = 1 + \frac{2}{3m}\beta^2 \quad (9)$$

(value of m as in eq 3) with $\langle R_e^2 \rangle$ and $\langle R_{e,0}^2 \rangle$ being the mean-square end-to-end distance in flow and at rest, respectively. In the regime of small deformations, the coil is assumed to still be Gaussian; i.e., the deformation ratios of $\langle R_e^2 \rangle$ and $\langle r_{gyr}^2 \rangle$ are approximately equal.[3,27]

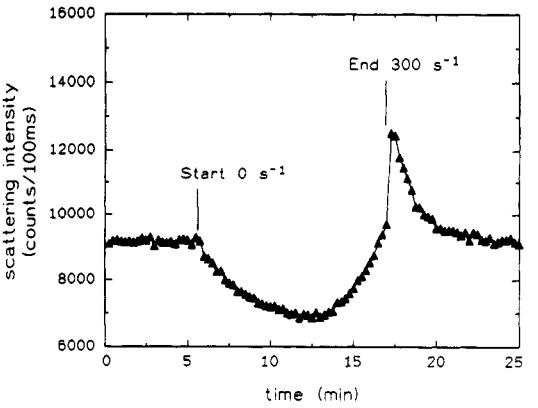

Figure 5. Scattering intensity of PS10 in DOP, $c = 0.113$ g/L, $T = 25$ °C, measured in the flow plane at $\omega = 120°$ and $\theta = 90°$.

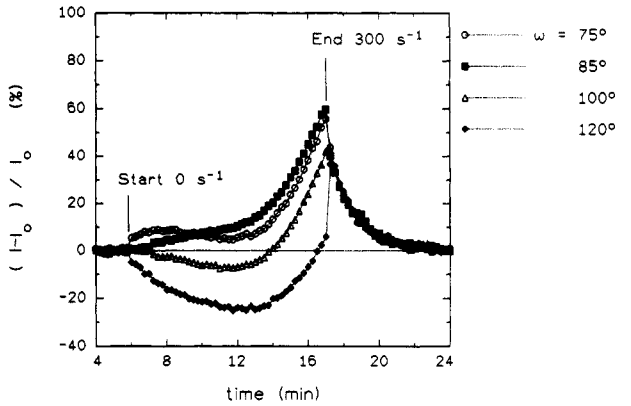

Figure 6. Relative scattering intensity at selected angles ω in the flow plane ($\theta = 90°$). Same sample as in Figure 5.

It should be stressed that the measurement method described above can only be performed if the detector range allows three-dimensional detection and if the orientation angle can be determined. With only one accessible detection plane, no more than two independent main radii of the gyration space can be determined. Without information about the orientation angle, the situations of the main gyration axes of the particle are not known, and therefore the contributions of $\langle S_A^2 \rangle$ and $\langle S_B^2 \rangle$ in $\langle S^2 \rangle$ cannot be distinguished. In the following we present the determination of the orientation angle and all three gyration radii of flow-oriented macromolecules.

Results

In all measurements the shear rate was increased linearly from zero up to the desired value, while the detector position was maintained.

Figure 5 shows the course of a typical LS measuring cycle in the flow plane beginning with a resting time of 6 min. From $t = 6$ min to $t = 17$ min the shear rate is increased linearly. A relaxation phase from $t = 17$ min to the end follows. This cycle was repeated for each measuring angle.

At the detector position shown in Figure 5, the scattering intensity decreases in the low shear region with increasing shear rate until $t = 13$ min. At other positions in the flow plane, scattering increases are also observed in this region, and in intermediate cases the scattering intensity does not change significantly. Figure 6 illustrates the relative scattering intensity at several positions in the flow plane, clearly showing the anisotropy of the scattering intensity under shear.

After cessation of shear, behavior is similar at all angles, but the initial intensity is reached only after a certain relaxation time. This is an unexpected finding since the

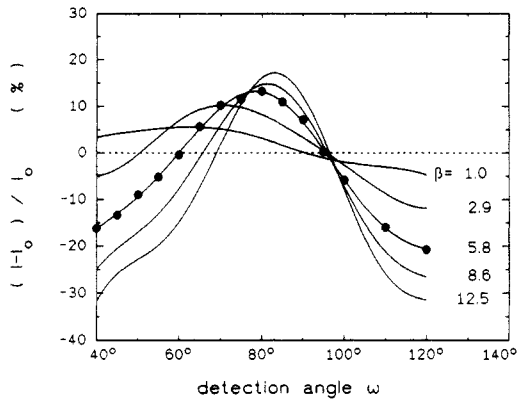

Figure 7. Relative intensity changes versus ω at different β for PS10 in DOP, c = 0.113 g/L, T = 25 °C.

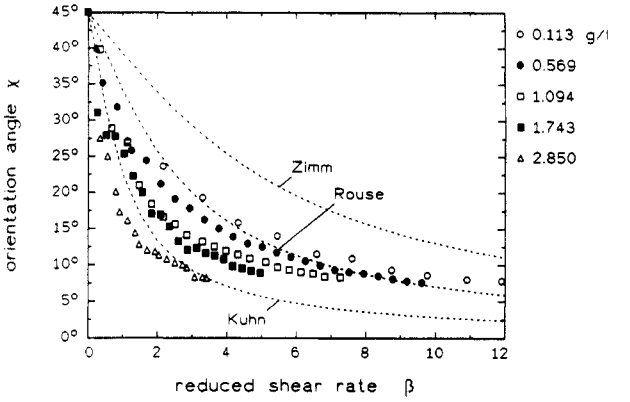

Figure 8. Orientation angles of PS10 in DOP, T = 25 °C. (Dashed lines denote theoretical values.)

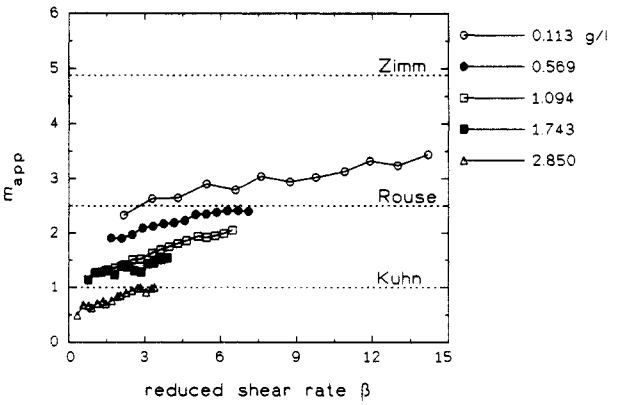

Figure 9. Apparent value of m of data in Figure 8 versus the shear parameter.

molecular relaxation time in the solution is 65 ms, as calculated from eq 1.

This relaxation process can be related to the strong scattering increase that begins at 180 s^{-1} (t = 13 min). The effect is present in the whole detection range. It was unequivocally identified as a shear-induced phase separation.[28-34] Some characteristics of our observations, which will be the subject of a separate publication, are mentioned here:

(i) The strong scattering increase occurs at all detector positions.

(ii) After stop of flow, a relaxation or redissolution time is needed to restore the scattering rate of quiescent solution. Then, the intensities before and after the experiment are equal to within experimental error (1–2%) for each solution, even after up to 50 measuring cycles.

(iii) If the critical shear rate for the onset of phase separation is not reached during the experiment, at shear stop the scattering intensity returns to the initial value within the molecular relaxation time (<100 ms).

(iv) With increasing polymer concentration, phase separation begins at lower shear rates.

(v) At elevated temperatures (30–55 °C) the effect sets in at higher shear rates, and the relaxation time after shear stop is shortened.

(vi) The Zimm extrapolations in the phase-separation regime (though distorted, see above) show rapidly increasing correlation length and molecular mass. The phase-separation region can therefore be distinguished well from the regime where only orientation and deformation effects occur.

As light scattering is a method essentially sensitive for particle size, the shear-induced phase separation can be detected in its very beginning and at very low concentrations ($c_{min} \approx 0.05$ g/L = 50 ppm).[33,34] However, in the following results the phase-separation regime will be disregarded.

Depolarization of the scattered light is an important point since the experimental conditions were similar to flow birefringence experiments, even though in comparison low concentrations and shear rates were used. Each investigated solution was checked, but a depolarization increase induced by shear was never detectable. Also, throughout all investigations no evidence of chain degradation by shear was found in the shear range used.[35]

Orientation. For the orientation angle determination from primary data like in Figure 6, relative intensity changes in the shear phase were plotted against the detection angle ω (Figure 7).

Compared to Figure 4, qualitatively the same picture is obtained. Each curve shows a maximum, with positions which move toward ω = 90°, while the maximum height increases. From eq 2, the orientation angle can be easily calculated.

Interestingly, all curves meet almost in one point on the zero line at $\omega \approx 95°$. Concerning this peculiarity, the results of Peterlin for the elastic dumbbell model[15] show a faint resemblance, whereas for the spring–bead model[16] he predicted an exact crosspoint of the relative scattering intensity curves located at ω = 90°. This may also serve as a qualitative test of the dynamic models and will be referred to later.

In Figure 8, orientation angles of a concentration series of PS10 in DOP together with the theoretical predictions (eq 3) are shown.

A concentration dependence is clearly revealed: the higher the concentration, the lower the orientation angles, i.e., the more complete the orientation process. At low concentrations, orientation data can be described approximately by the Rouse theory, whereas with increasing concentration, orientability increases and the orientation angles tend toward the Kuhn model. Exact information concerning this point is gained by plotting the apparent value of the parameter m from eq 10 for each data point

$$m_{app} = \beta \tan 2\chi \tag{10}$$

versus the reduced shear rate (Figure 9).

Linear dependences of m on concentration and on the shear parameter are revealed. The data were extrapolated to zero concentration, since none of the models considers intermolecular interactions. For $c \to 0$ a weak shear rate dependence of m results:

$$m = 2.1 + 0.1\beta \tag{11}$$

This can be interpreted as an increase of the particle's resistance with rising shear rate against further orientation,

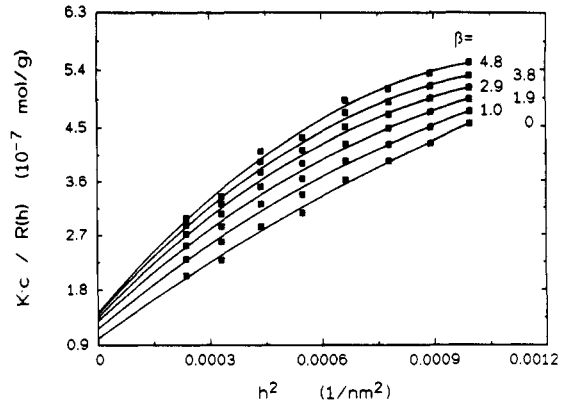

Figure 10. Zimm plot by variation of θ at $\omega = 140°$ on an intermediate concentration of PS10 in DOP, $c = 1.094$ g/L, $T = 25$ °C. Curves are polynominals of 2nd degree.

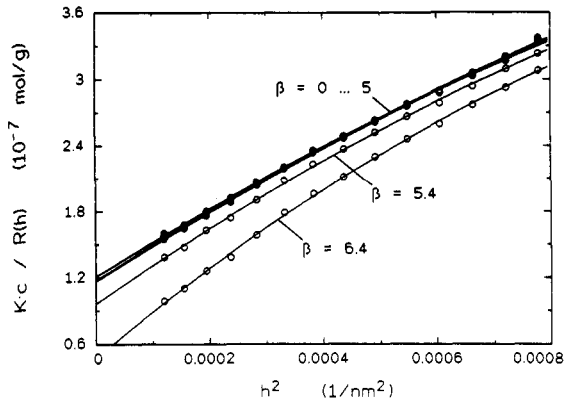

Figure 11. Zimm plot by θ variation at $\omega = 95°$ of PS10 in DOP, $c = 1.094$ g/L, $T = 25$ °C. Curves are polynominals of 2nd degree.

which is in contradiction to the prediction of a constant m value. The concentration dependence of the reduced steady-state compliance J_{eR} and the parameter m, which is the reciprocal of J_{eR}, is already known.[34] This has been established especially by flow birefringence, but no interpretation has been given yet. At least one can say that the presence of many oriented polymer coils increases the overall orientation degree, and the orientation resistance rises with increasing shear.

Deformation. Performing LS by angle variation on oriented particles, one should get a distorted Zimm plot, as is demonstrated in Figure 10.

For the deformation determination according to Peterlin,[14] three detector positions (ω,θ) were chosen. Though it should be irrelevant which (noncoplanar) positions are chosen, the ones where the scattering vector points approximately at the gyration main axes were preferred. As a consequence, each of the three positions was dominated by one of the gyration radii. Here, the measurement positions I(140°,90°), II(85°,90°), and III(90°,120°) were chosen.

Wavelength variation was performed by means of the Ar ion laser. Unfortunately, the λ range of the Ar ion laser is rather limited (458–514 nm) which causes uncertainty in the resulting Zimm extrapolations. Therefore, the zero-angle scattering rate was included in the extrapolations. In quiescent solution, for each solution the zero-angle scattering can be determined by angle variation. If the usual osmotic pressure virial expansion is limited to two coefficients which seems reasonable in a near-θ solvent, one can assume that

$$\frac{Kc}{R(0)} = \frac{1}{M_W} + 2A_2c = \text{constant}(q) \qquad (12)$$

supposing K and A_2 (=second osmotic virial coefficient)

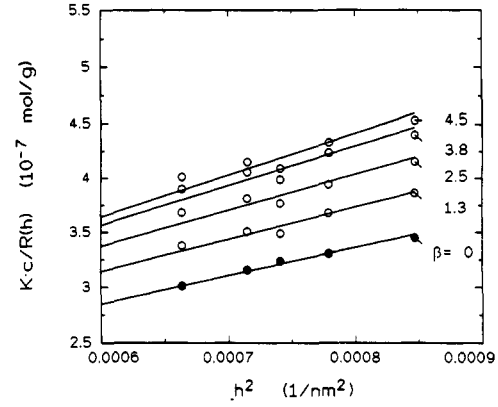

Figure 12. Zimm plot by wavelength variation at position I(140°, 90°) for PS10 in DOP, $c = 1.094$ g/L, $T = 25$ °C.

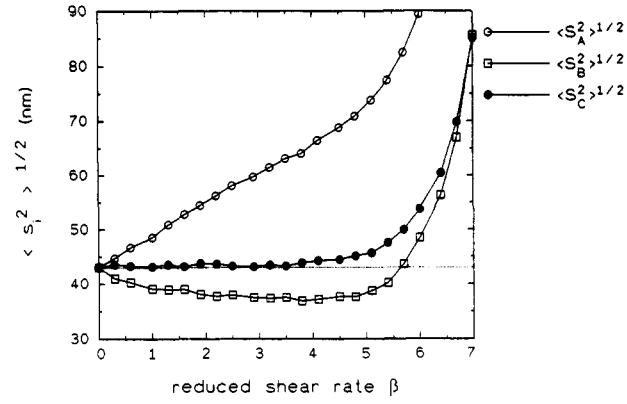

Figure 13. Main correlation lengths of PS10 in DOP depending on the shear parameter β, $c = 1.094$ g/L, $T = 25$ °C.

to be unaffected by the shear flow.

The validity of eq 12 was checked by performing θ variation under shear in the Zimm plane at $\omega = 95°$, because, due to the crosspoint in Figure 7, at $\omega = 95°$ almost undistorted Zimm extrapolations are possible. In this particular Zimm plane, no information converning the molecular deformation can be expected, but the value of the ordinate intercept $Kc/R(0)$ under shear can be determined well since the diagram is almost undistorted. $Kc/R(h=0,q)$ and $A_2(q)$ were investigated by this method for each solution and found to be constant to within experimental error (Figure 11; at $\beta = 5$ the phase-separation regime is entered).

Figure 12 shows a typical Zimm extrapolation by wavelength variation. For a first-order estimation of the deformation rates, linear fits were applied which meet in the common ordinate intercept. After evaluation of the local correlation lengths, the main correlation lengths of the molecular gyration space were calculated from eq 8, taking the previously determined orientation angles into account.

The resulting main correlation lengths are shown in Figure 13.

As predicted by theory, the longest correlation length ($\langle S_A^2\rangle^{1/2}$) expands while the short one in the flow plane ($\langle S_B^2\rangle^{1/2}$) decreases. The data for the third correlation length ($\langle S_C^2\rangle^{1/2}$) reflect remarkably well the theoretical result: within experimental errors, it is not affected by the flow. The same qualitative picture is yielded from all investigated concentrations. (When the phase-separation region is entered, all radii increase dramatically.)

Since also completely undeformable molecules would show a similar behavior for the three main radii (increase/decrease/constancy), only the mean radius of gyration indicates an actual deformation, that is, if it exceeds its value at rest. For this purpose, in Figure 14 the gyration

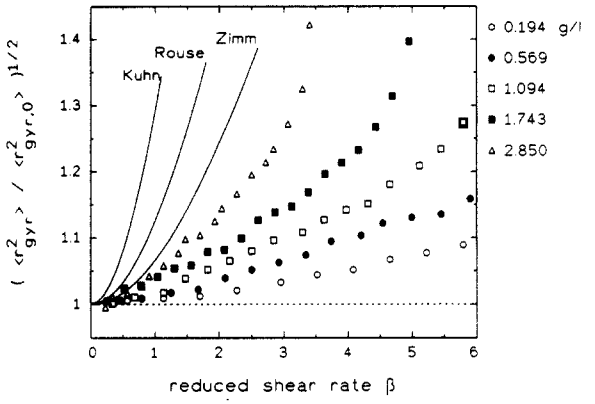

Figure 14. Deformation ratio of PS10 in DOP under flow against the shear parameter β, T = 25 °C.

radius extension ratio of some solutions of PS10 in DOP is plotted versus the reduced shear rate together with the theoretical results of Kuhn, Rouse, and Zimm.

In contrast to the orientation angles, a large discrepancy between theoretical and empirical deformation ratio is revealed. A striking feature of the curves is the strong dependence on concentration. With c = 2.85 g/L, the Zimm deformation ratio region is nearly reached. For the deformation ratio of PS10 in DOP, extrapolated to zero concentration, we found

$$\langle r_{gyr}^2\rangle/\langle r_{gyr,0}^2\rangle = 1 + (0.017 \pm 0.002)\beta^{1.40\pm0.05} \quad (13)$$

It should be stressed that the experimental data were recorded below the critical phase-separation shear rate, which was confirmed by the apparent molecular mass information from the Zimm plot by angle variation at ω = 95° (Figure 11). Figure 14 is surely the most important and also the most interesting result of our study.

Discussion

The shear-induced orientation angles determined from dilute solutions of high molar mass PS are in the range predicted by the theories of Kuhn, Rouse, and Zimm. A surprisingly strong concentration dependence and a weak β-dependence of the resistance parameter m is observed. The polymer concentrations were chosen from the lower limit suitable for LS (0.05–0.1 g/L) up to $c/c^* \approx 0.75$. Hence, at the higher concentrations, intermolecular interactions are certainly not negligible, which means that, in presence of many interacting polymer molecules, the orientation effect is augmented.

At very low concentration ($c \to 0$) and shear ($q \to 0$), the orientability is slightly higher than predicted by the Rouse model (eq 3). Most of the data points are situated between the models of Kuhn and Rouse. Moreover, the crosspoint in Figure 7 compared to the Peterlin results[15,16] confirms that the experimental data reflect a behavior between the Kuhn and the Rouse models. While flow birefringence[36] and dynamic viscosity measurements[37] of dilute polymer solutions usually show a rather Zimm-like behavior, it is known that Boger fluids[37] as investigated here may exhibit Rouse behavior.

This result may be due to the ultrahigh molar mass polymer or the very low concentrations used which is usually not the case in flow birefringence and dynamic viscosity measurements. Our current investigations on lower molar mass PS show a marked influence of molar mass on the extent of the concentration dependence of χ and m.[38]

Concerning the polydispersity of the polymer, Peterlin suggested a correction factor for β based on the Mark–Houwink law and the Schulz–Zimm molar mass distribution.[18] In our case, it leads to m_0 = 3.0 instead of 2.1 which at least means that the influence of polydispersity is comparatively great and should be considered, but it must be stated that a polydispersity correction has not always been applied in other experimental works.

The deformability of PS in DOP does not correspond to the scaling exponent of 2 as predicted by the theories (eq 13). Qualitatively, Cottrell, Merrill, and Smith[3] (CMS) have reported a similar result from their measurements on poly(isobutylene) in decalin. Their data describe an even lower deformability

$$\langle r_{gyr}^2\rangle/\langle r_{gyr,0}^2\rangle = 1 + 0.01\beta^{1.03} \quad (14)$$

taken from Figure 10 of ref 3. $\langle S_C^2\rangle$ was presumed to remain constant because it could not be measured.

In contrast to the qualitative coincidence with the results of CMS, we cannot confirm the finding of Lindner and Oberthuer (LO), that the deformation ratio of PS corresponds at least roughly to the theoretical predictions. One reason may be the fact that LO used orientation angle data of CMS, because with the flow SANS apparatus the determination of χ is not possible. However, the orientation angle is indispensable to calculate the main radii $\langle S_A^2\rangle^{1/2}$ and $\langle S_B^2\rangle^{1/2}$. Certainly, this work and the two others mentioned are not completely comparable since different polymers (CMS), solvents, and molar masses were investigated. The low deformability exponent of 1.40 found here is not affected by the Peterlin polydispersity correction; merely the prefactor is changed from 0.017 to 0.010.

In a recent paper, Menasveta and Hoagland[22] have reported light scattering from polystyrene in steady elongational flow. Surprisingly, also in elongational flow always a lower deformation was observed than predicted.[19–22] This fact is ascribed to the limited residence time of the individual molecules in the center of flow, which is a critical point in elongational flow techniques. Effects like this cannot be the reason for the behavior observed here. However, it appears that polymers generally show a much lower deformation than expected in any type of flow.[19,22]

The low deformations achieved in our measurements are probably the reason why no significant depolarization increase was observed.

DOP represents a near-θ solvent for PS. In general, the shear rate dependence of the intrinsic viscosity is less pronounced in poor solvents than in good solvents, as is known from viscosity measurements.[35] Orientation of polymer molecules lowers flow resistance and intrinsic viscosity, whereas deformation can be expected to increase the intrinsic viscosity.

The observed orientation angles reflect an orientability of the same magnitude as predicted. Hence, the measured Rouse-like orientability together with a very low deformability can be supposed to be one reason why highly dilute solutions of polymers also in θ-solvents show a shear rate dependence of the intrinsic viscosity. A direct comparison to viscosity measurements is desirable and will be given in a later publication.

Finally, it is clearly shown that LS from sheared polymer solutions yields a variety of interesting results: orientation angles and deformation ratio can be determined from dilute solutions. In addition, secondary flows[6] and shear-induced aggregation processes can be investigated very well with light scattering. In subsequent papers, we will report rheooptical measurements also in good solvents and on lower M_W polystyrenes.

Acknowledgment. We are greatly indebted to the "Deutsche Forschungsgemeinschaft" (DFG) for financial support as well as to Prof. Dr. Kiesewetter from the "Institut für Feinwerktechnik" of the Technical University Berlin for cooperation with the photometer construction, both within the framework of the "Sonderforschungsbereich 335 Anisotrope Fluide", Berlin. Special thanks to A. Wölfle and H. Stock, whose works made this study possible.

References and Notes

(1) Dupuis, D.; Layec, Y.; Wolff, C. *Optical Properties of Polymers*; Meeten, G. H., Ed.; Elsevier: New York, 1986; p 101.
(2) Heller, W.; Wada, E.; Papazian, L. A. *J. Polym. Sci.* **1960**, *47*, 481.
(3) Cottrell, F. R.; Merrill, E. W.; Smith, K. A. *J. Polym. Sci., Polym. Phys. Ed.* **1969**, *7*, 1415.
(4) Champion, J. V.; Davis, I. D. *J. Chem. Phys.* **1970**, *52*, 381.
(5) Ahmad, N.; Heller, W.; Nakagaki, M. *J. Colloid Interface Sci.* **1969**, *31*, 585.
(6) Cleschinsky, D.; Stock, H.; Springer, J. *Colloid Polym. Sci.* **1992**, *269*, 1250. Stock, H.; Zisenis, M.; Cleschinsky, D.; Springer, J. *Rheol. Acta* **1992**, *31*, 274. Link, A.; Zisenis, M.; Prötzl, B.; Springer, J. *Makromol. Chem., Macromol. Symp.* **1992**, *61*, 358.
(7) Lindner, P.; Oberthuer, R. C. *Rev. Phys. Appl.* **1984**, *19*, 759.
(8) Lindner, P.; Oberthuer, R. C. *Colloid Polym. Sci.* **1988**, *266*, 886.
(9) Bruns, W. *Colloid Polym. Sci.* **1976**, *254*, 325.
(10) Haller, W. *Kolloid-Z.* **1932**, *61*, 26.
(11) Kuhn, W. *Kolloid-Z.* **1934**, *68*, 2.
(12) Rouse, P. E. *J. Chem. Phys.* **1953**, *21*, 1272.
(13) Zimm, B. H. *J. Chem. Phys.* **1956**, *24*, 269.
(14) Peterlin, A. *J. Polym. Sci.* **1957**, *23*, 189.
(15) Peterlin, A.; Heller, W.; Nakagaki, M. *J. Chem. Phys.* **1958**, *28*, 470.
(16) Peterlin, A.; Reinhold, C. *J. Chem. Phys.* **1964**, *40*, 1029.
(17) Nakagaki, M.; Heller, W. *J. Chem. Phys.* **1976**, *64*, 3797.
(18) Peterlin, A. *J. Chem. Phys.* **1963**, *39*, 224.
(19) Smith, K. A.; Merrill, E. W.; Peebles, L. H.; Banijamali, S. H. *Colloq. Int. C.N.R.S.* **1975**, *233*, 341.
(20) Lumley, L. *Phys. Fluids* **1977**, *20*, 664.
(21) Cathey, Ch.; Fuller, G. G. *J. Non-Newtonian Fluid Mech.* **1990**, *34*, 63.
(22) Menasveta, M. J.; Hoagland, D. A. *Macromolecules* **1991**, *24*, 3427.
(23) Wölfle, A.; Springer, J. *Colloid Polym. Sci.* **1984**, *262*, 876.
(24) Schurz, J. *Introduction to Structure Rheology*; Verlag Berliner Union GmbH: Stuttgart, Germany, 1974.
(25) Taylor, G. I. *Proc. R. Soc. London* **1923**, *A102*, 541.
(26) Kuhn, W.; Kuhn, H. *Helv. Chim. Acta* **1943**, *26*, 1394.
(27) Cascales, J. J. L.; García de la Torre, J. *Macromolecules* **1990**, *23*, 809.
(28) VerStrate, G.; Philipoff, W. *J. Polym. Sci., Polym. Lett. Ed.* **1974**, *12*, 267.
(29) Wolf, B. A. *Macromolecules* **1984**, *17*, 615. Krämer-Lucas, H.; Schenck, H.; Wolf, B. A. *Makromol. Chem.* **1988**, *189*, 1613 and 1627.
(30) Rangel-Nafaile, C.; Metzner, A. B.; Wissbrun, K. F. *Macromolecules* **1984**, *17*, 1187.
(31) Onuki, A. *J. Phys. Soc. Jpn.* **1990**, *59*, 3427.
(32) Criado-Sancho, M.; Jou, D.; Casas-Vázquez, J. *Macromolecules* **1991**, *24*, 2834.
(33) Nakatani, A. I.; Waldow, D. A.; Han, C. C. *Polym. Mater. Sci. Eng.* **1991**, *65*, 216.
(34) Wu, X.-L.; Pine, D. J.; Dixon, P. K. *Phys. Rev. Lett.* **1991**, *66*, 2408.
(35) Odell, J. A.; Muller, A. J.; Narh, K. A.; Keller, A. *Macromolecules* **1990**, *23*, 3092. Brostow, W.; Ertepinar, H.; Singh, R. P. *Macromolecules* **1990**, *23*, 5109.
(36) Janeschitz-Kriegl, H. *Adv. Polym. Sci.* **1969**, *6*, 171.
(37) Bohdanecky, M.; Kovar, J. *Viscosity of Polymer Solutions*; Elsevier: New York, 1982.
(38) Prötzl, B.; Link, A.; Springer, J., in preparation.